Journal of Solid State Chemistry 184 (2011) 1882–1889

Contents lists available at ScienceDirect

Journal of Solid State Chemistry

journal homepage: www.elsevier.com/locate/jssc

Solid solubility of $Yb_2Si_2O_7$ in β-, γ- and δ-$Y_2Si_2O_7$

A.J. Fernández-Carrión [a], M.D. Alba [a], A. Escudero [b,1], A.I. Becerro [a,*]

[a] Instituto de Ciencia de Materiales de Sevilla (CSIC-Universidad de Sevilla), c/ Américo Vespucio, 49, 41092 Seville, Spain
[b] Bayerisches Geoinstitut, Universität Bayreuth, D-95440 Bayreuth, Germany

ARTICLE INFO

Article history:
Received 9 March 2011
Received in revised form
26 May 2011
Accepted 26 May 2011
Available online 2 June 2011

Keywords:
Rare earth silicates
$Y_2Si_2O_7$
$Yb_2Si_2O_7$
Solid solubility
Phase diagram

ABSTRACT

This paper examines the structural changes with temperature and composition in the $Yb_2Si_2O_7$–$Y_2Si_2O_7$ system; members of this system are expected to form in the intergranular region of Si_3N_4 and SiC structural ceramics when sintered with the aid of Yb_2O_3 and Y_2O_3 mixtures. A set of different compositions have been synthesised using the sol–gel method to obtain a xerogel, which has been calcined at temperatures between 1300 and 1650 °C during different times. Isotherms at 1300 and 1600 °C have been analysed in detail to evaluate the solid solubility of $Yb_2Si_2O_7$ in β-$Y_2Si_2O_7$ and γ-$Y_2Si_2O_7$. Although $Yb_2Si_2O_7$ shows a unique stable polymorph (β), Yb^{3+} is able to replace Y^{3+} in γ-$Y_2Si_2O_7$ and δ-$Y_2Si_2O_7$ at high temperatures and low Yb contents. IR results confirm the total solid solubility in the system and suggest a constant SiOSi angle of 180° in the Si_2O_7 unit across the system. The temperature–composition diagram of the system, obtained from powder XRD data, is dominated by the β-$RE_2Si_2O_7$ polymorph, with γ-$RE_2Si_2O_7$ and δ-$RE_2Si_2O_7$ showing reduced stability fields. The diagram is in accordance with Felsche's diagram if average ionic radii are assumed for the members of the solid solution at any temperature, as long as the β–γ phase boundary is slightly shifted towards higher radii.

1. Introduction

Rare Earth disilicates ($RE_2Si_2O_7$) exhibit different polymorphic forms depending on the *RE* ionic radius, temperature and pressure [1,2]. $Y_2Si_2O_7$ shows, in particular, up to five polymorphs with increasing temperature at room pressure (y, α, β, γ and δ, also called, respectively, y, B, C, D and E); while $Yb_2Si_2O_7$ exhibits a unique polymorph (β, also called C) up to the melting point of the compound. These silicates are important materials in the sinterization of the structural advanced ceramic Si_3N_4. It has been shown that when *RE* oxides (*RE*=lanthanides and yttrium), single or mixed, are added to the powder of pure Si_3N_4 as sintering aids, a glassy disilicate phase ($RE_2Si_2O_7$) forms in the intergranular regions, which, upon crystallisation, improves the high-temperature mechanical properties of the material [3,4]. Knowledge of the crystalline structures adopted by the $RE_2Si_2O_7$ intergranular phase at different temperatures and *RE* contents is therefore of great value in understanding the behaviour of these materials.

The aim of this research is to analyse the solid solubility of $Yb_2Si_2O_7$ in β-, γ- and δ-$Y_2Si_2O_7$ and to describe a temperature–composition diagram showing the polymorphism of the system. Study of the solid solubility of $Yb_2Si_2O_7$ in *y*- and α-$Y_2Si_2O_7$ is not reported due to the slow kinetics at the stability temperatures of these phases (<1200 °C) [5].

2. Experimental section

2.1. Synthesis of the xerogel

The following reactants have been used as starting materials: $Yb(NO_3)_3\cdot 5H_2O$ (99.99% Aldrich Chemical Co.), $Y(NO_3)_3\cdot 4H_2O$ (99.99% Aldrich Chemical Co.), $Si(OC_2H_5)_4$ (TEOS, 99% Aldrich Chemical Co.) and absolute ethanol (AnalaR Normapur). To verify the amount of water per formula unit present in the nitrates, thermogravimetric analyses (TGA) were carried out using a SDT Q600 (TA instruments). $Yb_{2-x}Y_xSi_2O_7$ members with nominal x=0.00, 0.40, 0.80, 1.00, 1.20, 1.40, 1.60, 1.80 and 2.00 were synthesised. A TEOS solution in ethanol (1:3 in volume) was added over the appropriate amounts of $Yb(NO_3)_3\cdot 5H_2O$ and $Y(NO_3)_3\cdot 4H_2O$ previously dissolved in 5 ml of absolute ethanol. The mixture was stirred at 40 °C for 5–7 h and the transparent gels obtained were dried at 60 °C for 24 h in air. Nitrates were eliminated by calcination at 500 °C for 2 h at a heating rate of 1 °C min^{-1}. Importantly, only a slight excess of TEOS in the initial mixture yielded satisfactorily the $Yb_{2-x}Y_xSi_2O_7$ phase, otherwise oxiorthosilicate phase was obtained in a large proportion.

2.2. Calcination experiments

The xerogel of each composition was ground in an agate mortar and subsequently divided into different portions, which

* Corresponding author. Fax: +34 954460665.
E-mail addresses: alberto.fernandez@icmse.csic.es (A.J. Fernández-Carrión), alba@icmse.csic.es (M.D. Alba), aescudero@icmse.csic.es (A. Escudero), anieto@icmse.csic.es (A.I. Becerro).
[1] Present address: Instituto de Ciencia de Materiales de Seville (CSIC- Universidad de Sevilla), c/ Américo Vespucio, 49, 41092 Sevilla, Spain.

0022-4596/$ - see front matter © 2011 Elsevier Inc. All rights reserved.
doi:10.1016/j.jssc.2011.05.034

were calcined in air at different temperatures between 1300 °C and 1650 °C and different periods of time (Table 1), using a heating rate of 5 °C min^{-1} and a platinum crucible. Finally, the samples were slowly cooled down to room temperature.

2.3. Characterisation

The global composition of the samples was examined by X-Ray fluorescence (Panalytical, AXIOS model). Table 2 shows the agreement between the nominal and real compositions.

An analytical transmission electron microscope (ATEM, Philips CM20FEG) operating at 200 kV and equipped with an energy-dispersive X-ray spectrometer (EDX, NORAN Ge detector) was used to observe the morphology of the samples as well as to examine chemical composition. The EDA software was used to index the electron diffraction patterns [6]. EDX analyses on $Yb_{2-x}Y_xSi_2O_7$ single crystals were carried out to determine yttrium and ytterbium contents. The quantification included an absorption correction and the calibration of Cliff–Lorimer factors for ytterbium and yttrium with respect to silicon, determined from pure $Yb_2Si_2O_7$ and $Y_2Si_2O_7$, respectively. At least 10 rare earth disilicate single crystals were analysed in each sample to calculate the mean compositions (results are displayed in third column of Table 2). A counting time from 100 to 300 s has been used in order to accumulate enough X-ray counts. The samples were dispersed in ethanol by sonication and dropped on a conventional carbon-coated copper grid.

X-Ray diffraction patterns (PANalytical XPert Pro Diffractometer, Cu$K\alpha$ and X-Celerator detector) were recorded over the angular range $10^\circ < 2\theta < 120^\circ$ 2θ with step width of 0.02° and 10 s counting time. The patterns were analysed using the Rietveld method with the TOPAS software (TOPAS version 4.2, Bruker AXS 2009). Refined parameters were background coefficients, zero correction, scale, unit cell parameters, site occupation factors for the rare earth sites, isotropic atomic displacement parameters, atomic positions and microstructure parameters.

Finally, Infrared Fourier Transform spectra (Nicolet 510 FTIR instrument equipped with DTGS detectors) were recorded over the 1500–400 cm^{-1} range with a resolution of 2 cm^{-1}. The measurements were made using dried KBr pellets, which were prepared by mixing and pressing 1.5 mg of sample with 100 mg KBr.

Table 1
Polymorphs obtained after calcination of the $Yb_{(2-x)}Y_xSi_2O_7$ compositions at different temperatures and times.

T (°C)	t (h)	0.00	0.40	0.80	1.00	1.20	1.40	1.60	1.80	1.94	2.00
1300	24	β	β	β	β	β		β			β
1400	12										β
	36										γ+β
	72						β	β+γ	β+γ		
1500	24							β+γ	β+γ		γ+(β)
1550	24						β+γ	β+γ			
	48						γ	γ			
1600	24		β	β	β	β	β+γ				
	36										γ
	48							γ+β			
	63.2							γ			
1650	12					β	γ+β	γ	γ	γ+δ	γ+δ
	24					β+γ	γ	γ	γ		γ+δ

Table 2
Compositional data obtained with different techniques for $Yb_{2-x}Y_xSi_2O_7$ samples.

× Nominal	× FRX	× Rietveld		× EDX/TEM
		β	γ	
0.00	0.00	0.00 (0.00)	–	0.00
0.40	0.35	0.36 (0.01)	–	0.40
0.80	0.81	0.80 (0.01)	–	0.85
1.00	1.00	1.00 (0.01)	–	0.96
1.20	1.21	1.26 (0.01)	–	Non-recorded
1.40	Non-recorded	–	1.40 (0.01)	Non-recorded
1.60	1.59	1.64 (0.01)	1.58 (0.03)	1.61
1.80	Non-recorded	–	1.81 (0.01)	Non-recorded
2.00	2.00	2.00 (0.00)		2.00

3. Results and discussions

3.1. Solid solubility of $Yb_2Si_2O_7$ in β-$Y_2Si_2O_7$: Study of the 1300 °C isotherm

3.1.1. X-ray diffraction study

Representative portions of the XRD patterns of different $Yb_{2-x}Y_xSi_2O_7$ members calcined at 1300 °C for 24 h are shown in Fig. 1. The diagram of the $x=0.0$ sample matches the standard pattern of pure β-$Yb_2Si_2O_7$ (PDF 00-025-1345), as expected. Increasing Y content produces very similar patterns, with slight variations in peak positions and intensity; see, for example, the shift of the peaks under the dashed lines, the intensity decrease in the

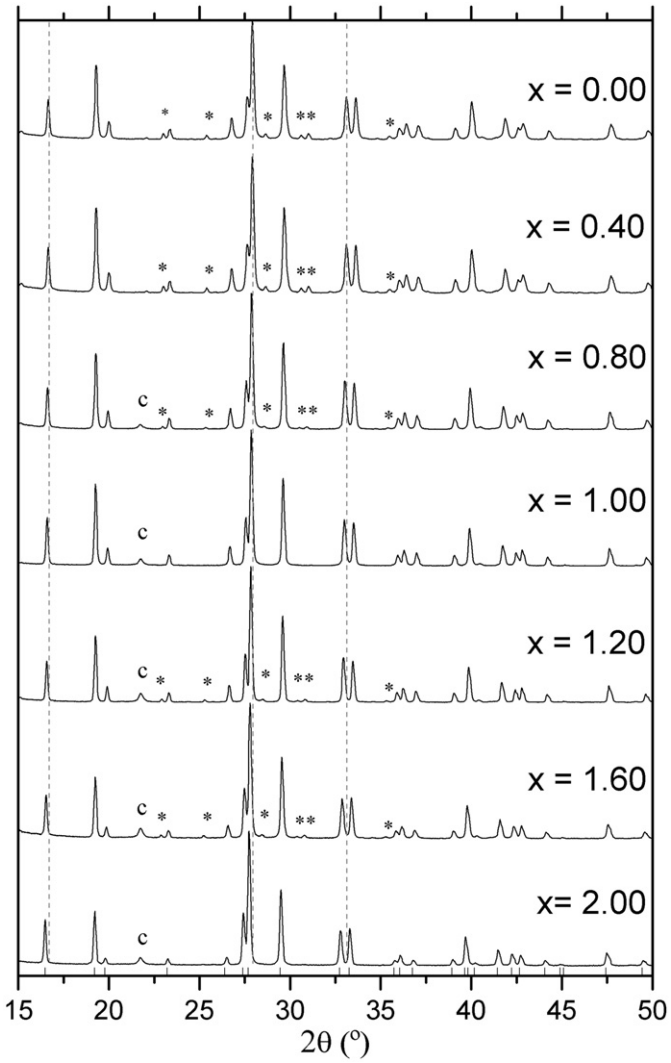

Fig. 1. Selected portions of the XRD patterns of $Yb_{2-x}Y_xSi_2O_7$ samples annealed at 1300 °C for 24 h. Asterisks: X2-RE_2SiO_5; c: cristobalite. Dashed lines are guides to the eye to show shift of reflections with composition.

diffraction at ~20° 2θ and the progressive resolution of the double reflection ~42.5° 2θ. This fact results from variations in unit cell dimensions and composition. Yb^{3+} is smaller than Y^{3+} (ionic radius in octahedral coordination = 0.868 and 0.900 Å, respectively) [7] and they have different atomic form factor curves. At the other end of the series, the diagram of the $x=2.0$ sample matches the standard pattern of β-$Y_2Si_2O_7$ (JCPDS card 00-038-0440). The structure of the β-polymorph is, therefore, maintained across the $Yb_2Si_2O_7$–$Y_2Si_2O_7$ system at 1300 °C. Some weak reflections corresponding to X2-RE_2SiO_5 (marked with asterisks) and cristobalite (marked with c) can be observed in some compositions.

The XRD patterns of all $Yb_{2-x}Y_xSi_2O_7$ compositions calcined at 1300 °C were analysed using the Rietveld method with the TOPAS software, as described in Section 2. The starting parameters for the refinement of the structures with $x \leq 1$ have been taken from those reported for pure β-$Yb_2Si_2O_7$ [8] while the refinement of the structures with $x > 1$ was carried out from the parameters reported for pure β-$Y_2Si_2O_7$ [9]. Additionally, the oxyorthosilicate and cristobalite phases were included in the refinements. Fig. 2 exhibits the experimental, fitted and difference curves obtained from the refinement of the $x=0.40$ composition. The rest of compositions show very similar fits to this one and are not shown. It can be observed that all the reflections could be fitted on the basis of a monoclinic unit cell with space group $C2/m$, as corresponds to the crystal structure of the β-$RE_2Si_2O_7$ polymorph. Table 3 shows the atomic parameters obtained for the $x=0.40$ composition, together with the percentage of $(Yb,Y)_2SiO_5$ impurity and the fit statistics. Atomic parameters for the rest of compositions are supplied as supplementary information.

Fig. 3 shows the unit cell parameters as a function of Y content. The same size of the y-axis has been used in the plots of a, b and c unit cell parameters in order to appreciate relative changes. Both a and b unit cell parameters increase linearly with increasing Y content, while c unit cell parameter does not change appreciably with composition. The β-angle of the unit cell decreases linearly with increasing Y content, while the unit cell volume increases linearly. The unit cell parameters behaviour in the system β-$Yb_2Si_2O_7$–β-$Y_2Si_2O_7$ indicates the formation of a complete solid solution from β-$Yb_2Si_2O_7$ to β-$Y_2Si_2O_7$ at 1300 °C. This behaviour is qualitatively very similar to other thortveitite systems, such as β-$Lu_2Si_2O_7$–β-$Y_2Si_2O_7$ [10] and β-$Lu_2Si_2O_7$–β-$Sc_2Si_2O_7$ [11].

Finally, the Y and Yb occupations of the unique rare earth site of the thortveitite structure, obtained from the Rietveld refinements, are displayed in Table 2. A good agreement is observed between these occupations and the nominal composition of the samples.

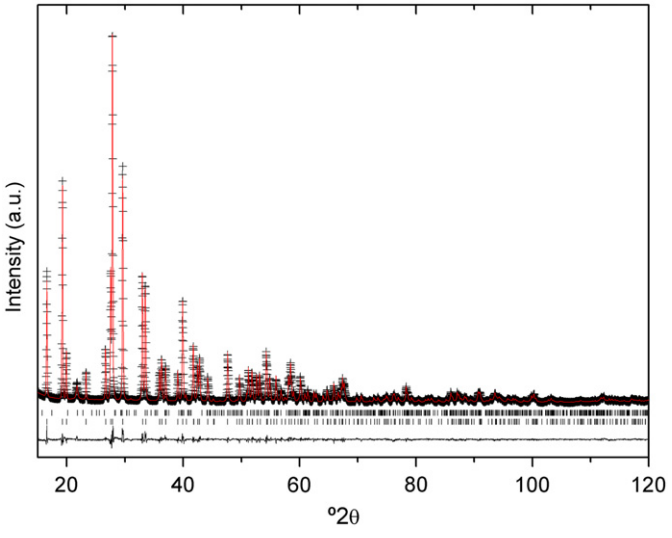

Fig. 2. Experimental (crosses), fitted (line) and difference curves obtained from the refinement of β-$Yb_{1.6}Y_{0.40}Si_2O_7$ using space group $C2/m$. Bottom tick marks: $(Yb,Y)_2Si_2O_7$; top tick marks: X2-$(Yb,Y)_2SiO_5$.

Table 3
Refined atomic coordinates for $Yb_{1.6}Y_{0.4}Si_2O_7$ from X-ray powder diffraction data collected at RT (space group $C2/m$; $a=6.8162(2)$ Å, $b=8.8932(2)$ Å, $c=4.7101(1)$ Å, $\beta=101.95(1)°$). Impurities present: 6% $(Yb,Y)_2SiO_5$. Fit statistics—R_{wp}: 7.62, R_p: 5.74, R_{Bragg}: 2.67.

Site	x	y	z	Occ.	B_{eq}
Yb1	0.5	0.8065(1)	0.0000	0.82(1)	0.87(4)
Y	0.5	0.8065(1)	0.0000	0.18(1)	0.87(4)
Si1	0.7190(4)	0.5	0.4135(6)	1	0.50(8)
O1	0.5	0.5	0.5	1	1.10(22)
O2	0.8689(8)	0.5	0.6980(11)	1	0.60(16)
O3	0.7284(6)	0.6441(4)	0.2291(7)	1	0.60(13)

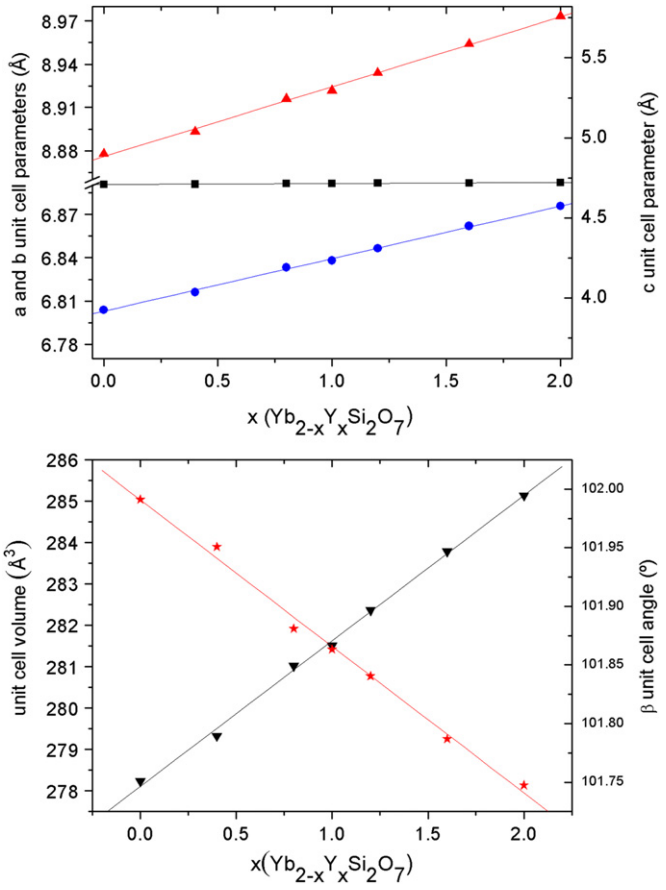

Fig. 3. Unit cell parameters of $Yb_{2-x}Y_xSi_2O_7$ samples annealed at 1300 °C (β-$RE_2Si_2O_7$ polymorph) as a function of composition. Top figure: Circles, up triangles and squares—a, b and c unit cell parameters, respectively. Bottom figure: Down triangles and stars—unit cell volume and beta unit cell angle, respectively. The error bars are approximately the size of the symbols.

3.1.2. TEM study

Fig. 4A shows a representative TEM micrograph of different grains of the $Yb_{2-x}Y_xSi_2O_7$ ($x=1.00$) sample calcined at 1300 °C. The typical morphology of the grains consists of rounded particles with irregular borders, as expected from high temperature calcination. The electron diffraction pattern of the grain marked with an arrow in Fig. 4A is shown in Fig. 4B. The observed reflections on the SAED pattern are compatible with monoclinic symmetry and $C2/m$ space group, which is the one corresponding to the β-$RE_2Si_2O_7$ structure. This pattern can be indexed according to the

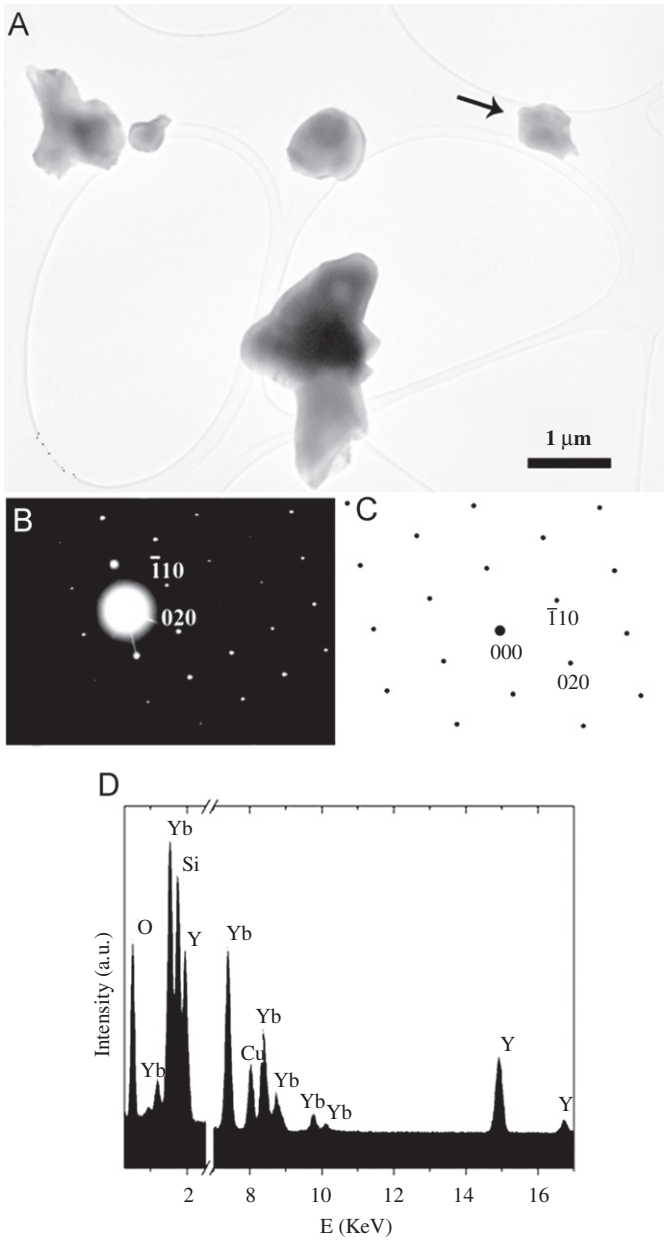

Fig. 4. (A) TEM micrograph of rare earth disilicate grains in the $Yb_{1.0}Y_{1.0}Si_2O_7$ sample synthesised at 1300 °C. (B) Electron diffraction pattern of the disilicate single crystal marked with an arrow in (A), compatible with β-$YbY_2Si_2O_7$ along the [0 0 1] zone axis. (C) Simulation of the SAED pattern of β-$RE_2Si_2O_7$ along the [0 0 1] zone axis (space group $C2/m$). (D) EDX spectrum of the same grain.

β-$RE_2Si_2O_7$ [0 0 1] zone axis, as observed in the simulation presented in Fig. 4C. The EDX spectrum of the single crystal of Fig. 4A is shown in Fig. 4D; it shows the characteristic X-ray emissions lines of Yb, Y and Si, demonstrating the simultaneous presence of both Yb and Y atoms in the single-crystal. The EDX spectra of other single crystals of this sample are very similar to the one presented in Fig. 4D, indicating a high degree of chemical homogeneity. After a very careful examination, only one of the studied grains showed a SAED pattern compatible with SiO_2 cristobalite (not shown), in agreement with the XRD pattern shown above.

The same behaviour is observed in the rest of the $Yb_{2-x}Y_xSi_2O_7$ compositions. Single crystals of disilicate also show X-ray emissions lines of Yb, Y and Si, with different intensity ratio depending on the nominal sample composition. This indicates solid solubility in the whole $Yb_{2-x}Y_xSi_2O_7$ system. The results of the EDX quantification for Yb and Y carried out on disilicate single crystals of different $Yb_{2-x}Y_xSi_2O_7$ compositions are presented in Table 2. A good agreement between the nominal and measured compositions is observed.

3.1.3. IR study

The IR spectra of the samples in the $Yb_{2-x}Y_xSi_2O_7$ system annealed at 1300 °C are shown in Fig. 5. The spectrum of the sample with $x=2.00$ is in agreement with that published by Diaz et al. [12] for β-$Y_2Si_2O_7$. The spectra of the rest of compositions in the $Yb_{2-x}Y_xSi_2O_7$ system are similar to the one of pure β-$Y_2Si_2O_7$, the only appreciable difference being the position of the signals marked with asterisk in the figure. The bands in the IR spectrum of β-$Y_2Si_2O_7$ were assigned to 18 vibrational modes [12]. The 1100–1077 cm^{-1} band corresponds to stretching vibrations of silicon atoms against oxygen atoms in Si–O–Si bonds, ν_{as}SiOSi. The remaining high-frequency modes correspond to Si–O stretching motions involving apical (nonbridging) oxygens. The lower frequency modes are more difficult to characterize, because single Y–O and Si–O vibrations coexist in similar spectral ranges [13,14]. It was stated that the modes from 600 to 500 cm^{-1} are mainly due to Y–O stretching, and those from 500 to 400 cm^{-1} are modes with a large component of Si–O bending. It is remarkable that the absence of observable bands in the spectral region 600–800 cm^{-1} of any composition ascribed to the ν_sSiOSi mode in bent disilicate anions. This mode is absent in the infrared spectra of linear disilicate anions as there is no dipole change involved. This fact suggests, therefore, a value of 180° for the SiOSi angle of the Si_2O_7 unit across the β-$Yb_2Si_2O_7$ to β-$Y_2Si_2O_7$ system. However, in spite of that this mode was not observed in the β-$Sc_2Si_2O_7$–β-$Y_2Si_2O_7$ related system, where ^{29}Si and ^{89}Y Magic Angle Spinning Nuclear Magnetic Resonance (MAS-NMR) spectra revealed a value of the SiOSi angle < 180° for the intermediate compositions [15,16]. Due

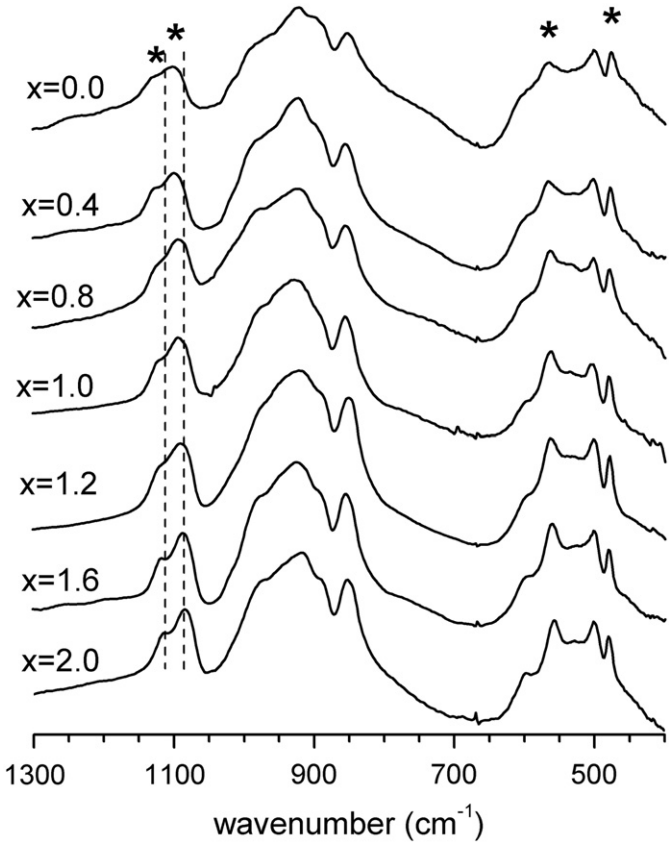

Fig. 5. IR spectra of $Yb_{2-x}Y_xSi_2O_7$ samples calcined at 1300 °C. The υ_{as}SiOSi, Y–O stretching and Si–O bending vibrational modes have been marked with asterisks.

to the paramagnetic nature of Yb^{3+}, NMR spectra cannot be recorded on the members of the β-$Yb_2Si_2O_7$–β-$Y_2Si_2O_7$ to check the SiOSi angle across this system. However, the υ_{as} (Si–O–Si) band located in the 1100–1077 cm^{-1} region of the IR spectra could provide some additional information. The analysis of the evolution of the maximum with composition either will help confirm the linearity of the SiOSi bond suggested by the non-observation of the v_sSiOSi mode or will inform the variation of that angle with composition.

Lazarev [17] showed that the wavenumber of the υ_{as} mode was determined by the SiOSi bond angle and by the electronegativity of the groups (R and OR′) directly bounded to the silicon, $R_3Si–OR'$. Both factors influence the pπ–dπ interaction between Si and O, therefore increasing the force constant, $K_{Si–O}$. The vibration frequency increases as a consequence of a polarity change of the σ–SiO bond.

The group electronegativity sum of a given Q'' silicon site is determined as follows [18]:

$$\sum EN(Q^n) = \sum EN(\mathrm{OSi}) + (4-n)\sum \left(EN_{\mathrm{nf}} z_{\mathrm{nf}} / \sum z_{\mathrm{nf}}\right) \quad (1)$$

where n represents the total number of framework tetrahedra coordinated to a given silicon tetrahedron. In our case, $n=1$ because we are dealing with pyrosilicate structures. EN_{nf} represents the group electronegativity value for nonframework ligands, and z_{nf} is the formal charge of a nonframework cation. In the case of $Y_xYb_{2-x}Si_2O_7$, the group electronegativity sum of the Si site is obtained by adding the group electronegativities of the four groups bonded to the silicon as follows:

$$\sum EN(Q^1) = EN(\mathrm{OSi}) + \frac{3}{2}(xEN(\mathrm{OY}) + (2-x)EN(\mathrm{OYb})) \quad (2)$$

To obtain electronegativity values of groups of atoms, like OSi, OY and OYb, Hual et al. [19] proposed that the group electronegativity should be equalized within the margin of groups belonging to the centres of positive and negative charges or within groups belonging to the symmetry centres. Therefore, the electronegativity of a group AB, EN(AB), should be

$$EN(\mathrm{AB}) = \frac{\sum n_i}{\sum \frac{n_i}{x_i}} \quad (3)$$

where n_i is the number of atoms or smaller groups in group AB and x_i is the electronegativity of an atom or smaller group.

Fig. 6a shows the relationship between the υ_{as} band position and the group electronegativity sum of the silicon site in a set of β-$RE_2Si_2O_7$ compounds (RE=Sc, Lu, Y and Yb), calculated using Eqs. (2) and (3). Three of the compounds show a linear relationship (R^2=0.93) between both parameters, given by the following equation:

$$\upsilon_{as} = 429.064 + 83.964\sum EN(Q^1) \quad (4)$$

while $Yb_2Si_2O_7$ does not fit the line. According to Eqs (2) and (4) and using the υ_{as} value obtained from the IR spectrum of $Yb_2Si_2O_7$ (Fig. 5a), the EN(OYb) should be 1.860, while the calculation from Eq. (3) using the Pauling electronegativity of Yb gives 1.667. To clarify this disagreement, the Pauling electronegativity values of the lanthanide elements have been plotted against Z in Fig. 6b. A linear relationship (R^2=0.96) is observed, given by the following equation:

$$X_p = 0.41069 + 0.0122Z \quad (5)$$

which is in good agreement with the periodic character of this property, with the exception, again, of Yb. The Pauling electronegativity of Yb has been recalculated from Eq. (5) and it has been used to calculate the actual EN(OYb) using Eq. (3). This calculation gives EN(OYb)=1.849, which is close to 1.860.

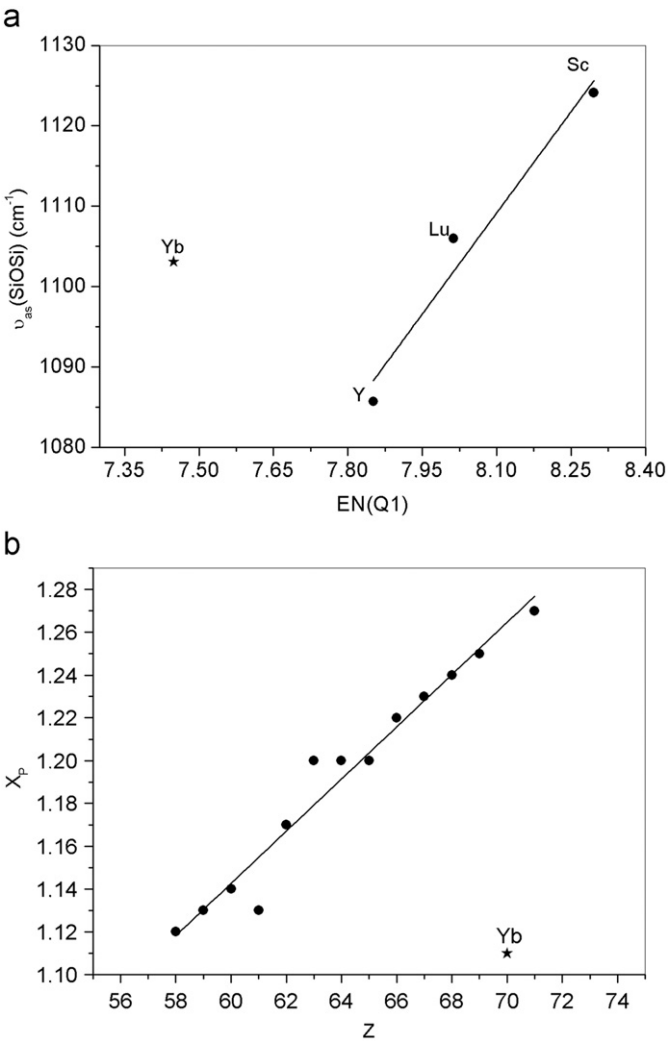

Fig. 6. (a) Plot of υ_{as}(SiOSi) frequency vs. total electronegativity of Si in different β-$RE_2Si_2O_7$ compounds (RE=Lu, Sc, Y and Yb) and (b) plot of Pauling electronegativity of lanthanides vs. atomic number Z.

The group electronegativity sums of Si in the β-$Yb_{2-x}Y_xSi_2O_7$ system have been calculated using the recalculated EN(YbO) value. The position of the υ_{as} band has been plotted vs. the electronegativity sums of Si (Fig. 7), and a linear correlation (R^2=0.98) has been obtained, given by the following equation:

$$\upsilon_{as} = 120.34 + 122.87\sum EN(Q^1) \quad (6)$$

This linear relationship confirms the solid solubility of $Yb_2Si_2O_7$ in β-$Y_2Si_2O_7$ in the whole compositional range, from a short range order point of view. This fact, together with the absence of the υ_s SiOSi band, suggests that there is no change in the SiOSi angle across the $Yb_2Si_2O_7$–β-$Y_2Si_2O_7$ system.

3.2. Solid solubility of $Yb_2Si_2O_7$ in γ-$Y_2Si_2O_7$: Study of the 1650 °C isotherm

3.2.1. XRD study

Fig. 8 shows the XRD patterns of the samples with $x \geq 1.40$ calcined at 1650 °C for 24 h. The patterns are very similar to each other and match the PDF 00-042-0167 corresponding to γ-$Y_2Si_2O_7$, with slight variations in peak positions and intensities resulting from changes in unit cell dimensions and contents. No reflections corresponding to β-$Yb_2Si_2O_7$ are observed for these

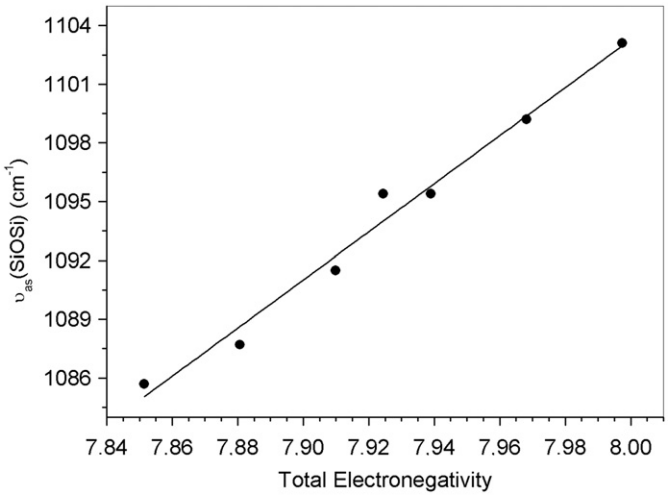

Fig. 7. Plot of υ_{as}(SiOSi) frequency taken from Fig. 5 vs. total electronegativity of Si in β-$Y_xYb_{2-x}Si_2O_7$ (x=0.00–2.00).

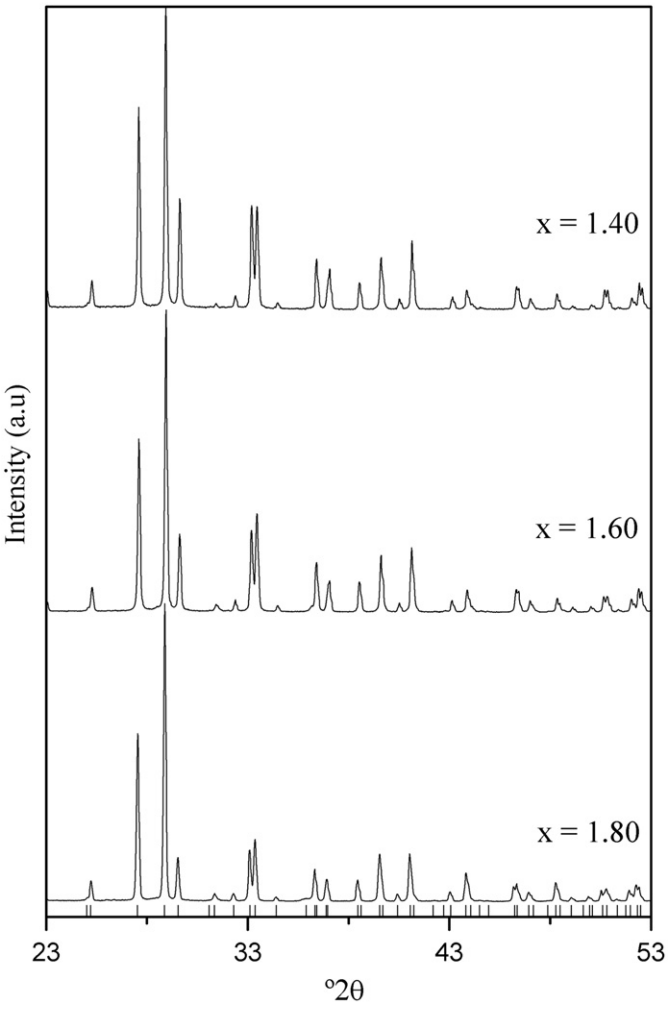

Fig. 8. Selected portions of the XRD patterns of $Yb_{2-x}Y_xSi_2O_7$ samples with $x \geq 1.40$ calcined at 1650 °C for 24 h. Tick marks correspond to reflections of γ-$Y_2Si_2O_7$ (PDF 00-042-0167).

compositions. Therefore, β-$Yb_2Si_2O_7$ does not segregate from $Y_2Si_2O_7$ but a unique phase γ-$RE_2Si_2O_7$ is formed in the compositional range $1.40 \leq x \leq 1.80$ at 1650 °C. This fact indicates that even

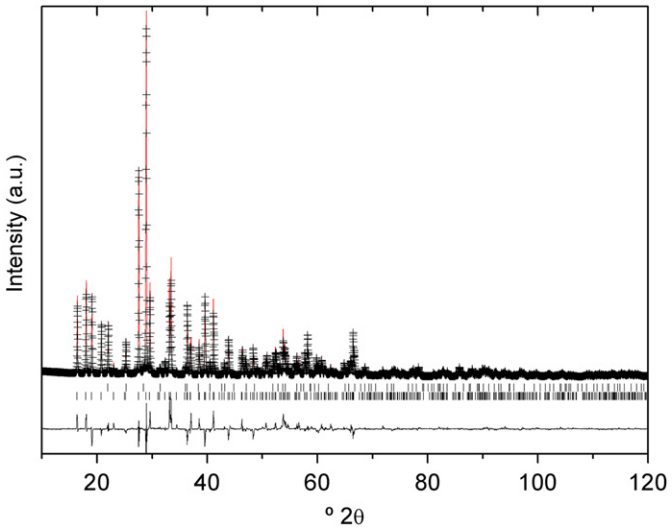

Fig. 9. Experimental (crosses), fitted (line) and difference curves obtained from the refinement of γ-$Yb_{0.4}Y_{1.60}Si_2O_7$ using space group $P2_1/c$. Bottom tick marks: γ-$Yb_{0.4}Y_{1.60}Si_2O_7$. Top tick marks: Cristobalite.

though pure $Yb_2Si_2O_7$ crystallises as β-$Yb_2Si_2O_7$ at any temperature [2] there is some degree of solid solubility of $Yb_2Si_2O_7$ in γ-$Y_2Si_2O_7$.

To confirm the solid solubility of $Yb_2Si_2O_7$ in γ-$Y_2Si_2O_7$ a Rietveld refinement was performed for compositions $1.40 \leq x \leq 1.80$ annealed at 1650 °C. Fig. 9 shows the experimental, fitted and difference curves obtained from the refinement of γ-$Yb_{0.4}Y_{1.60}Si_2O_7$. Cristobalite was added as secondary phase (less than 6% in all compositions). The rest of fits are very similar and are not shown. All reflections could be fitted on the basis of a monoclinic unit cell with space group $P2_1/c$, corresponding to the crystal structure of the γ-rare earth disilicates [20]. Unit cell parameters as a function of composition are shown in Fig. 10. Values of the unit cell parameters corresponding to pure γ-$Y_2Si_2O_7$ (sample annealed at 1600 °C) have also been plotted. The same size of the y-axis has been used in the three plots to appreciate relative changes in a, b and c parameters. Both b and c unit cell parameters increase linearly with increasing Y content, while the a unit cell parameter does not change appreciably with composition. The β angle of the unit cell decreases with increasing Y content, and the unit cell volume increases linearly. The linear behaviour of the unit cell parameters with composition is a clear indication of the solid solubility of $Yb_2Si_2O_7$ in γ-$Y_2Si_2O_7$ in the compositional range $1.40 \leq x \leq 2.00$ at high temperature.

Finally, the Y and Yb occupations of the unique rare earth site of the γ-$RE_2Si_2O_7$ structure in the corresponding stability range, obtained from the Rietveld refinements, are displayed in Table 2. A good agreement is observed between these occupations and the nominal composition of the samples.

3.2.2. TEM study

The incorporation of Yb in the structure of γ-$Y_2Si_2O_7$ has been analysed by TEM-EDX. Fig. 11A shows a representative micrograph of several grains of the $Yb_{0.2}Y_{1.8}Si_2O_7$ sample. The electron diffraction pattern of the grain marked with an arrow in Fig. 11A appears in Fig. 11B. This pattern is compatible with the γ-$Y_2Si_2O_7$ [0 0 1] zone axis, as inferred from the simulation presented in Fig. 11C. The EDX spectrum of this single crystal (Fig. 11D) shows the characteristic X-ray emissions lines of Y and Si and also some low intensity peaks corresponding to Yb. This demonstrates the incorporation of ytterbium into γ-$Y_2Si_2O_7$ at high temperature and high yttrium content.

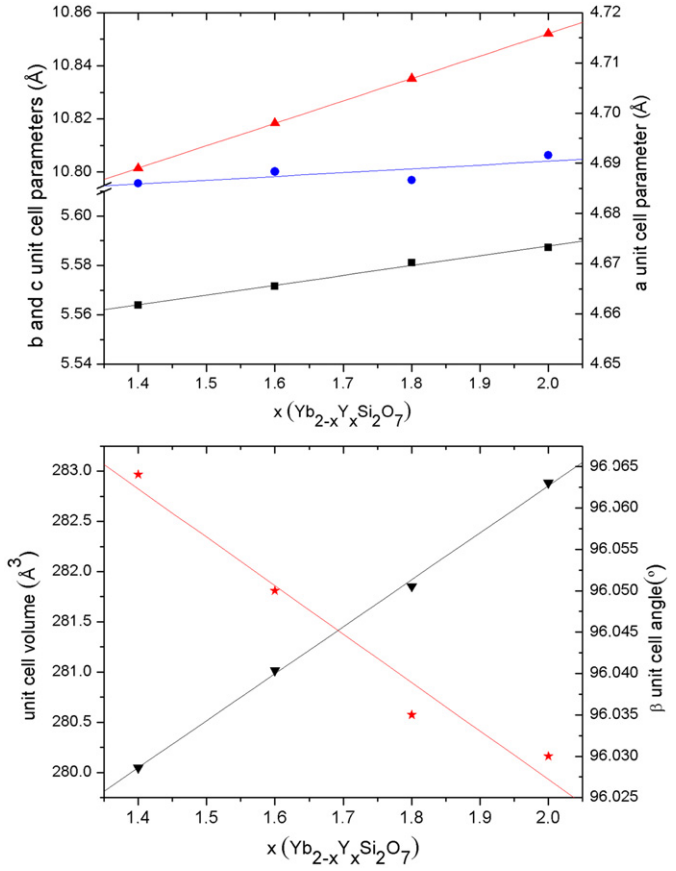

Fig. 10. Unit cell parameters of $Yb_{2-x}Y_xSi_2O_7$ samples annealed at 1650 °C (γ-$RE_2Si_2O_7$ polymorph) as a function of composition. Top figure: Circles, up triangles and squares—*a*, *b* and *c* unit cell parameters, respectively. Bottom figure: Down triangles and stars—unit cell volume and beta unit cell angle, respectively. The error bars are approximately the size of the symbols.

3.3. $Yb_2Si_2O_7$–$Y_2Si_2O_7$ phase diagram

Once the solid solubility of $Yb_2Si_2O_7$ in β- and γ-$Y_2Si_2O_7$ has been demonstrated, additional calcinations were carried out in order to determine the phase boundaries among the different polymorphs. Limitation in the maximum temperature of our furnace has hindered carrying out an exhaustive analysis of the solid solubility of $Yb_2Si_2O_7$ in δ-$Y_2Si_2O_7$, and only transition temperatures for some Y-rich compositions have been determined to eventually draw the corresponding phase boundary.

The behaviour of the $Yb_{2-x}Y_xSi_2O_7$ members with $1.00 \leq x \leq 2.00$ calcined at temperatures ≥ 1300 °C for different times has been summarised in Table 1. Compositions with $x \leq 1.00$ show, exclusively, the β-$RE_2Si_2O_7$ polymorph after calcination at any temperature. The member with $x=1.20$ crystallises as β-polymorph at temperatures < 1650 °C and the XRD pattern shows some reflections of γ-$RE_2Si_2O_7$ after annealing at 1650 °C for 24 h. The $x=1.40$ member behaves in a similar manner, although transition to the γ polymorph is observed after 24 h annealing at 1550 °C. The XRD pattern of the $x=1.60$ composition shows reflections of both the β- and γ-polymorphs after calcination at 1400 °C for 72 h; pure γ-$RE_2Si_2O_7$ is observed after calcination at higher temperatures and longer times. The $x=1.80$ member shows partial transformation to the γ-polymorph after calcination at 1400 °C for 72 h. The $x=1.94$ annealed at 1650 °C for 12 h shows mainly reflections of γ-$RE_2Si_2O_7$ together with some low intensity reflections of the δ-polymorph. Finally, the XRD pattern of the Y-rich end-member ($x=2.00$) annealed at 1400 °C for 36 h shows reflections indicative of partial β to γ-$Y_2Si_2O_7$ transformation.

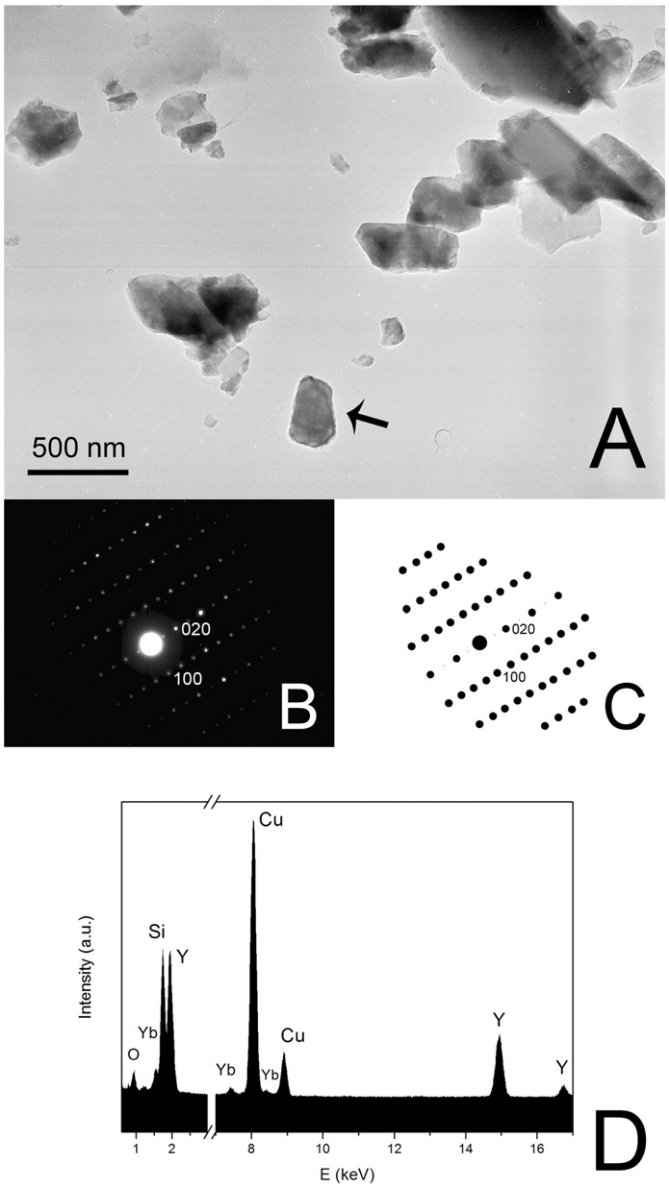

Fig. 11. (A) TEM micrograph of grains corresponding to the $Yb_{0.2}Y_{1.8}Si_2O_7$ sample annealed at 1650 °C. (B) Electron diffraction pattern of the grain marked with an arrow in (A). (C) Simulation of the electron diffraction pattern of γ-$Y_2Si_2O_7$ along the [0 0 1] zone axis. Grey spots correspond to not-allowed γ-$Y_2Si_2O_7$ reflections that could be observed in the experimental diffraction pattern due to double diffraction phenomena. (D) EDX spectrum of the grain marked with an arrow in (A).

All the data presented above have been summarised in Fig. 12a, which represents the polymorphism in the temperature–composition phase diagram of the $Yb_2Si_2O_7$–$Y_2Si_2O_7$ system. The diagram is dominated by the β-$RE_2Si_2O_7$ polymorph, displaying more reduced stability fields in γ- and δ-polymorphs. The diagram is similar to those previously reported for the $Lu_2Si_2O_7$–$Y_2Si_2O_7$ system [21] and the $Sc_2Si_2O_7$–$Y_2Si_2O_7$ system [15]. The three systems share one end-member ($Y_2Si_2O_7$) while the other end-member ($Lu_2Si_2O_7$, $Sc_2Si_2O_7$ and $Yb_2Si_2O_7$) shows exclusively the β polymorph at any temperature. Therefore, the similarity between the temperature–composition diagrams is not surprising. The main difference between them is the width of the β-field, which shows the smaller area in the $Yb_{2-x}Y_xSi_2O_7$ system and the maximum one

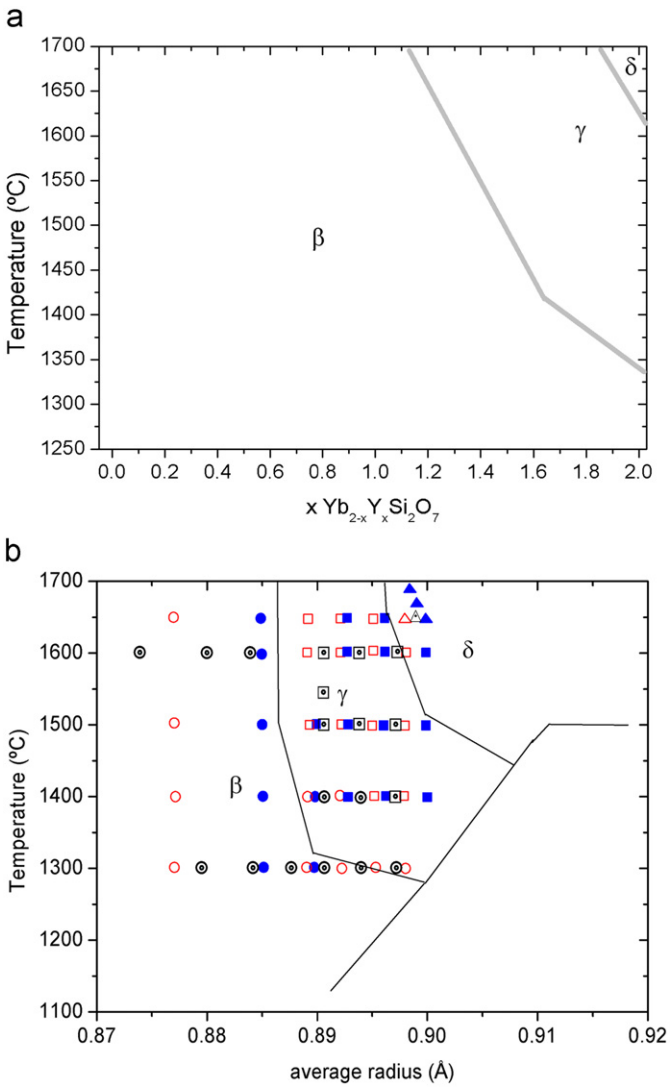

Fig. 12. (a) Temperature–composition diagram of the $Yb_2Si_2O_7$–$Y_2Si_2O_7$ system as a function of temperature and composition. (b) Polymorphism, as a function of average radii, in the systems $Yb_2Si_2O_7$–$Y_2Si_2O_7$ (dotted symbols), $Lu_2Si_2O_7$–$Y_2Si_2O_7$ (solid symbols) [21] and $Sc_2Si_2O_7$–$Y_2Si_2O_7$ (open symbols) [15] compared to phase boundaries of Felsche [2] for pure rare earth disilicates. Circles: β-$RE_2Si_2O_7$. Squares: γ–$RE_2Si_2O_7$. Triangles: δ-$RE_2Si_2O_7$.

in the $Sc_{2-x}Y_xSi_2O_7$ system, showing the $Lu_{2-x}Y_xSi_2O_7$ system an intermediate value. Pomeroy et al. (2005) [22] suggested that the phase stabilities of a disilicate solid solution behave just like the phase stabilities of a silicate with *RE* ionic radius equal to the average of the radii of the rare earths in the solid solution ("radius criterion"). In Fig. 12b all experimentally determined phase stabilities have been plotted versus the average of the radii of the rare earths in the three solid solutions. In addition, the phase stability boundaries of Felsche [2] have been plotted in the diagram. Most of the polymorphs of the three systems are in accordance with this radius criterion, although, in view of the stability phases observed at 1300 and 1400 °C, it seems that the $\beta-\gamma$ phase boundary should be slightly shifted to higher radii. Therefore, a prediction of phase stabilities of solid solutions of rare-earth disilicates is possible according to Felsche's diagram [2] if average ionic radii are assumed, as long as the β–γ phase boundary is slightly shifted towards higher radii. However, it is important to note that partial solid solutions of rare-earth disilicates that do not have any polymorph in common might not obey to this simple rule (e.g. the $La_2Si_2O_7$–$Y_2Si_2O_7$ system [23]).

4. Conclusions

$Yb_2Si_2O_7$ and $Y_2Si_2O_7$ form a complete solid solution at 1300 °C showing the β-$RE_2Si_2O_7$ modification. In addition, $Yb_2Si_2O_7$, which shows a unique polymorph (β-$Yb_2Si_2O_7$) up to the melting point, is soluble in γ- and δ-$Y_2Si_2O_7$ at low Yb contents and high temperatures. The temperature–composition diagram of the $Yb_2Si_2O_7$–$Y_2Si_2O_7$ system is dominated by the β-$RE_2Si_2O_7$ polymorph, and is in accordance with Felsche's diagram if average ionic radii are assumed for the members of the solid solution, as long as the β–γ phase boundary is slightly shifted towards higher radii. This shift is also valid for other rare earth disilicate systems.

Acknowledgments

A.J. Fernandez-Carrion gratefully acknowledges an F.P.D.I. grant from Junta de Andalucía. Supported by DGICYT (Project no. CTQ2010-14874/BQU), Junta de Andalucía (FQM-6090) and the Leibniz programme of the Deutsche Forschungsgemeinschaft (LA 830/14-1 to FL).

Appendix A. Supplementary materials

Supplementary data associated with this article can be found in the online version at doi:10.1016/j.jssc.2011.05.034.

References

[1] J. Ito, H. Johnson, Am. Mineral. 53 (1968) 1940.
[2] J. Felsche, Struct. Bond. 13 (1973) 99.
[3] Z.L. Hong, et al., J. Eur. Ceram. Soc. 22 (2002) 527.
[4] S. Kurama, I. Schulz, M. Herrmann, J. Eur. Ceram. Soc. 29 (2009) 155.
[5] A. Escudero, A.I. Becerro, J. Phys. Chem. Solids 68 (2007) 1348.
[6] T. Kogure, J. Crystallogr. Soc. Jpn. 45 (2003) 391.
[7] R.D. Shannon, C.T. Prewitt, Acta Crystallallogr. B 26 (1970) 1046.
[8] A.N. Christensen, Z. Kristallogr. 209 (1994) 7.
[9] G.J. Redhamer, G. Roth, Acta Crystallogr. C 59 (2003) 1103.
[10] A.I. Becerro, A. Escudero, J. Solid State Chem. 178 (2005) 1.
[11] H. Ohashi, M.D. Alba, A.I. Becerro, P. Chain, A. Escudero, J. Phys. Chem. Solids 68 (2007) 464.
[12] M. Diaz, C. Pecharroman, F. del Monte, J. Sanz, J.E. Iglesias, J.S. Moya, C. Yamagata, S. Mello-Castaño, Chem. Mater. 17 (2005) 1774.
[13] Y. Repelin, C. Proust, E. Husson, J.M. Beny, J. Solid State Chem. 118 (1995) 163.
[14] A.M. Hofmeister, A. Chopelas, Phys. Chem. Miner. 17 (1991) 503.
[15] A. Escudero, M.D. Alba, A.I. Becerro, J. Solid State Chem. 180 (2007) 1436.
[16] M. Allix, M.D. Alba, P. Florian, A.J. Fernandez-Carrion, M. Suchomel, A. Escudero, E. Suard, A.I. Becerro, J. Appl. Crystallallogr., 2011, in press, doi:10.1107/S0021889811021303.
[17] A.N. Lazarev (Ed.), Vibrational Spectra and Structure of Silicates, Consultants Bureau, New York, 1972.
[18] N. Janes, E. Oldfield, J. Am. Chem. Soc. 107 (1985) 6169.
[19] L. Hual, W. Qingwel, L. Lixin, J. Chem. Educ. 69 (1992) 783–784.
[20] A.N. Christensen, R.G. Hazell, A.W. Hewat, Acta Chem. Scand. 51 (1997) 37.
[21] A.I. Becerro, A. Escudero, J. Eur. Ceram. Soc. 26 (2006) 2293.
[22] M.J. Pomeroy, E. Nestor, R. Ramesh, S. Hampshire. J. Am. Ceram. Soc. 88 (2005) 875.
[23] A.J Fernández-Carrión, A. Escudero, M. Suchomel, A.I. Becerro. In preparation.